Please cite this article in press as: Vahabikashi et al., Probe Sensitivity to Cortical versus Intracellular Cytoskeletal Network Stiffness, Biophysical Journal (2019), https://doi.org/10.1016/j.bpj.2018.12.021

Biophysical *Journal*
Article

Biophysical Society

Probe Sensitivity to Cortical versus Intracellular Cytoskeletal Network Stiffness

Amir Vahabikashi,[1] Chan Young Park,[2] Kristin Perkumas,[3] Zhiguo Zhang,[2] Emily K. Deurloo,[2] Huayin Wu,[4] David A. Weitz,[4,5,6] W. Daniel Stamer,[3,7] Robert D. Goldman,[8] Jeffrey J. Fredberg,[2] and Mark Johnson[1,9,10,*]

[1]Department of Biomedical Engineering, Northwestern University, Evanston, Illinois; [2]Department of Environmental Health, Harvard T.H. Chan School of Public Health, Boston, Massachusetts; [3]Department of Ophthalmology, Duke University, Durham, North Carolina; [4]School of Engineering and Applied Sciences, Harvard University, Cambridge, Massachusetts; [5]Wyss Institute for Biologically Inspired Engineering, Harvard University, Cambridge, Massachusetts; [6]Department of Physics, Harvard University, Cambridge, Massachusetts; [7]Department of Biomedical Engineering, Duke University, Durham, North Carolina; [8]Department of Cell and Molecular Biology, Feinberg School of Medicine, Northwestern University, Chicago, Illinois; [9]Department of Ophthalmology, Feinberg School of Medicine, Northwestern University, Chicago, Illinois; and [10]Department of Mechanical Engineering, Northwestern University, Evanston, Illinois

ABSTRACT In development, wound healing, and pathology, cell biomechanical properties are increasingly recognized as being of central importance. To measure these properties, experimental probes of various types have been developed, but how each probe reflects the properties of heterogeneous cell regions has remained obscure. To better understand differences attributable to the probe technology, as well as to define the relative sensitivity of each probe to different cellular structures, here we took a comprehensive approach. We studied two cell types—Schlemm's canal endothelial cells and mouse embryonic fibroblasts (MEFs)—using four different probe technologies: 1) atomic force microscopy (AFM) with sharp tip, 2) AFM with round tip, 3) optical magnetic twisting cytometry (OMTC), and 4) traction microscopy (TM). Perturbation of Schlemm's canal cells with dexamethasone treatment, α-actinin overexpression, or RhoA overexpression caused increases in traction reported by TM and stiffness reported by sharp-tip AFM as compared to corresponding controls. By contrast, under these same experimental conditions, stiffness reported by round-tip AFM and by OMTC indicated little change. Knockout (KO) of vimentin in MEFs caused a diminution of traction reported by TM, as well as stiffness reported by sharp-tip and round-tip AFM. However, stiffness reported by OMTC in vimentin-KO MEFs was greater than in wild type. Finite-element analysis demonstrated that this paradoxical OMTC result in vimentin-KO MEFs could be attributed to reduced cell thickness. Our results also suggest that vimentin contributes not only to intracellular network stiffness but also cortex stiffness. Taken together, this evidence suggests that AFM sharp tip and TM emphasize properties of the actin-rich shell of the cell, whereas round-tip AFM and OMTC emphasize those of the noncortical intracellular network.

INTRODUCTION

Biomechanical properties of cells influence a variety of basic cellular behaviors, including migration, proliferation, contraction, elongation, adhesion, cytokinesis, and apoptosis (1–3). These behaviors in turn impact tissue morphogenesis, cancer metastasis, bronchospasm, vasospasm, systemic hypertension, glaucoma, and atherosclerosis (4–10). Early studies of cellular biomechanics considered the cell to be either a homogeneous structure or a fluid-like cytoplasm surrounded by a cortical elastic shell. It is now clear, however, that the mechanical behavior of a cell is determined by the structure of the cortical, intracellular (noncortical) cytoskeletal, and nuclear networks (11,12), their distribution in space, and the complex rheology of the cytoplasm and cytosol (13). How these factors are reflected by different experimental probes, however, remains unclear.

We examine here the cytoskeletal mechanics of endothelial cells of the inner wall of Schlemm's canal (SC) cells, with possible relevance to glaucoma (14,15). To expand the generality of the results and to focus on the role of vimentin, we also consider mouse embryonic fibroblasts (MEFs). Experiments employed atomic force microscopy (AFM) with both sharp and round tips, optical magnetic twisting cytometry (OMTC), and traction microscopy (TM). Each of these probes provides complementary characterization of the material properties of these cells, with AFM tips measuring resistance to indentation (12), OMTC measuring the resistance of the cells to applied torque (16), and TM characterizing the

Submitted May 16, 2018, and accepted for publication December 20, 2018.

*Correspondence: m-johnson2@northwestern.edu

Editor: Jochen Guck.

https://doi.org/10.1016/j.bpj.2018.12.021

Please cite this article in press as: Vahabikashi et al., Probe Sensitivity to Cortical versus Intracellular Cytoskeletal Network Stiffness, Biophysical Journal (2019), https://doi.org/10.1016/j.bpj.2018.12.021

active tensile component in the cells (17). These are surface probes that would be expected to be influenced by the stiffness of the F-actin dense cortical region of the cell, which we refer to here as the cortex, and by the intracellular cytoskeleton but not by the much softer cytoplasm/cytosol (11,18).

We found that for all manipulations to both cell types, sharp-tip AFM probes and TM gave similar characterization of cell biomechanical behavior and were sensitive primarily to the cortical region of the cell. In contrast, larger round-tip AFM probes and OMTC were sensitive to both the cortical and intracellular network but primarily the latter. Finally, the absence of vimentin caused a reduction in stiffness of both the cortical and intracellular networks and in cellular traction.

MATERIALS AND METHODS

Cell isolation and culture

SC cells were isolated and cultured from postmortem enucleated human eyes within 36 h of death with enucleation occurring less than 6 h after death (15). Eyes with history of trabeculoplasty, anterior segment surgery, or any ocular disease (except cataract) were excluded. SC cells between passages three and five were used for all experiments. SC cells were characterized by established procedures (expression of vascular endothelial cadherin, net transendothelial electrical resistance of 10 $\Omega \cdot cm^2$ or greater, and lack of myocilin induction by dexamethasone (15)). SC cells were cultured in Dulbecco's modified Eagle's medium/low glucose (Life Technologies, Grand Island, NY) with 10% fetal bovine serum (Atlanta Biologicals, Norcross, GA) and 1% penicillin/streptomycin (Life Technologies).

Wild-type (WT) and vimentin knockout (KO) MEFs were originally extracted from mouse embryo and immortalized as discussed previously (19). MEFs were cultured in Dulbecco's modified Eagle's medium/high glucose (Life Technologies) supplemented with 10% fetal calf serum (Atlanta Biologicals), 5 mM nonessential amino acids (Life Technologies), and 1% penicillin/streptomycin (Life Technologies). MEFs were either sparsely seeded or confluent when tested.

All cell cultures were maintained in a humidified incubator at 5% CO_2 and 37°C, and media were changed every other day. Cells were passaged when they were around 80% confluent. For passaging, cells were washed with phosphate-buffered saline (PBS) (Life Technologies) to remove the serum, then treated with trypsin-EDTA 0.25% (Thermo Fischer Scientific, Grand Island, NY) and passaged at a ratio of 1:3.

Cell cultures were examined under various conditions of confluency: superconfluent, confluent, or sparsely confluent.

Dexamethasone studies

Stock solutions of dexamethasone (0.01, 0.1, and 1 mM; Sigma Aldrich, Milwaukee, WI) were prepared in ethanol as the vehicle and then diluted with culture medium to final concentrations of 0.01, 0.1, and 1 μM dexamethasone. Control studies used the same ethanol concentration (1%) as used in the dexamethasone solutions. Two normal SC cell strains (SC71, SC76) were treated with dexamethasone or control solutions for 7 days because it takes this long to get a reliable dexamethasone response (20). Media were replaced every other day. Cells were superconfluent at the end of the treatment.

Overexpression of α-actinin and RhoA expression

Four normal (SC69, SC71, SC73, SC76) cell strains were transduced with 1) an adenovirus encoding a ubiquitin promoter driving GFP, 2) a ubiquitin promoter driving α-actinin with a GFP tag, or 3) a ubiquitin promoter driving RhoA with a GFP tag; a fourth group 4) consisting of non-transduced cells (no virus) was also used. Groups 1 and 4 served as controls. Cells were confluent when tested.

AFM measurements

All AFM measurements were made with cells in media with 10% fetal bovine serum. AFM measurements were made on a BioScope II with Nanoscope V controller (Bruker, Santa Barbara, CA) coupled to an inverted fluorescent microscope with 10× (NA = 0.3) and 20× (NA = 0.8) objective lens (Carl Zeiss, Thornwood, NY). Sharp tips were pyramidal cantilevers mounted on a triangular cantilever with a length of 200 μm, a nominal tip radius of 20 nm, a tip half angle of 20° (as measured using scanning electron microscopy), and a nominal spring constant of 0.02 N/m (Olympus TR400PSA; Asylum Research, Goleta, CA). We note that the tip half angle was less than the nominal value reported by the manufacturer (36°). Round tips were spheres of 10 μm diameter mounted on silicon nitride cantilevers with nominal spring constant of 0.01 N/m (Novascan Technologies, Ames, IA). Indentation depths were between 100 and 400 nm, which we have previously shown to give values of cellular Young's modulus (E) that were relatively independent of indentation (12) while also avoiding any substrate effects (21). Measurements were done on regions well away from both nucleus and cell edges. Young's modulus was determined as described in the Supporting Materials and Methods (12). AFM measurements are done in this study with a ramp of 800 nm/s; we have previously shown (12) that this speed is sufficiently slow such that our measurements are not rate dependent, and that with the algorithm used (21), elastic modulus is relatively independent of indentation and load (12). The spring constant was calibrated before each experiment using the thermal fluctuations function of the nanoscope, which measures the motion of cantilever in response to thermal noise. Typically, 10–40 AFM measurements were made per each experimental condition. For AFM measurement of cells transduced with α-actinin, the microscope fluorescent mode was used to locate transduced cells with the GFP tag, followed by AFM measurements on those cells; for cells transduced with RhoA, the fluorescent tag was difficult to visualize in our AFM system, and thus this step was not taken before AFM measurements. However, transfection was separately confirmed using fluorescent microscopy and Western blotting (22).

OMTC measurements

Cells were seeded to 96-well plates (Corning, Corning, NY) in the presence of 10% serum. Ferromagnetic beads (4.5 μm in diameter), coated with poly-L-lysine, were allowed to attach to the cells for 20–30 min (14). The beads were then magnetized with a strong magnetic pulse in the horizontal direction and twisted with a much weaker oscillatory magnetic field (0.77 Hz) in the vertical direction. The torque on the bead was automatically adjusted to achieve a median bead translation of ~40 nm, and bead motion was quantified by image analysis. The ratio of magnetic torque to bead motion was used to determine complex shear modulus of cells, and the elastic modulus, g', which has units of pascals per nanometer, was used as a measure of cell stiffness as previously described (14,23).

TM measurements

Cells were seeded on collagen-coated acrylamide gels in 96-well plates or 35 mm glass-bottomed dishes in the presence of 10% serum (media for each cell type as described above) throughout the experiments. The gels were prepared as previously described (24) and had a Young's modulus of 8 kPa for SC cells and confluent MEFs and 2.4 kPa for sparsely seeded MEFs. A Leica epifluorescence microscope (Leica, Wetzlar, Germany) was used to take images of fluorescent microparticles on acrylamide gels. Based upon these images, displacements made by cells on gel were

Please cite this article in press as: Vahabikashi et al., Probe Sensitivity to Cortical versus Intracellular Cytoskeletal Network Stiffness, Biophysical Journal (2019), https://doi.org/10.1016/j.bpj.2018.12.021

calculated using particle image velocimetry (25), and from the displacement fields, traction was retrieved using Fourier transform TM (25,26). For confluent and superconfluent cells, root mean-square traction was used as a measure of average cellular contractile force (24), and for sparsely seeded cells, the contractile moment was used as a measure of average cellular contractile force (26).

Confocal imaging

Cells were seeded onto glass cover slips 48 h before fixation and stained for confocal experiments. 100% methanol (Sigma) was used as the fixative for experiments in which vimentin was the only cytoskeletal filament to be stained (Mendez et al. (27)). For all other experiments, 4% paraformaldehyde (Electron Microscopy Sciences, Hatfield, PA) was used (pH 7.4). Methanol fixation was done by incubating cells with precooled methanol for 10 min inside a −20°C freezer, and for paraformaldehyde fixation, cells were fixed for 10 min at room temperature. For cases in which the secondary antibody was raised in goat (p-myosin and vimentin staining), samples were blocked in 10% normal goat serum (Life Technologies) for 20 min to block for the nonspecific binding before incubation with primary antibody. For all other cases, cells were incubated with Image-iT FX Signal Enhancer (Life Technologies) for 20 min before incubation with primary antibody.

For dexamethasone experiments, cells were stained for F-actin (30 min incubation with Alexa Fluor 568 Phalloidin; Life Technologies), vimentin (30 min incubation with Alexa Fluor 488 Conjugated Vimentin (D21H3) XP Rabbit monoclonal antibody; Cell Signaling Technology, Danvers, MA), the nucleus (15 min incubation with Hoechst 33342 (1:10,000); Thermo Fischer Scientific), and p-myosin (overnight incubation at 4°C with Phospho-Myosin Light Chain 2, Ser19 (1:100), followed by two washes with PBS and 1 h incubation with goat anti-rabbit IgG (H + L) Alexa Fluor 488 (1:400); Cell Signaling Technology). For RhoA and α-actinin experiments, cells were stained for F-actin (30 min incubation with Alexa Fluor 568 Phalloidin) and the nucleus (15 min incubation with Hoechst 33342 (1:10,000)).

A Zeiss 510 laser scanning microscope inverted two-photon confocal microscope equipped with 10× (NA = 0.3), 20× (NA = 0.8), 40× (water immersion, NA = 1.2), and 63× (oil immersion, NA = 1.4) objective lenses and excitation sources of Ar (458, 488, 514 nm), HeNe (543 nm), HeNe (633 nm), and 2-photon (690–1024 nm) was used to create confocal images from the samples (Carl Zeiss). Thickness of MEFs and fluorescent intensity for the peripheral F-actin and p-myosin for SC cells were measured using Fiji image processing software.

Bead-embedding depths were examined in WT and KO MEFs by using a confocal microscope (Leica TSC SP5, 63×/1.2 NA water immersion lens; Leica) after staining cytoplasm with a fluorescent dye (Cell-Tracker Green; Thermo Fisher) (28). Using ImageJ, the percentage of bead embedding was quantified (29).

SIM

MEFs were fixed with 3% paraformaldehyde, permeabilized with 0.1% Triton-X100 (Sigma Aldrich) in PBS for 10 min at room temperature, and then rinsed briefly in PBS. The samples were subsequently incubated in chicken anti-vimentin antibody (1:2000; Biolegend, San Diego, CA) in PBS containing 5% normal goat serum (Jackson Immuno Research, West Grove, PA) for 30 min at room temperature, followed by washing with PBS containing 0.05% Tween 20 twice for 3 min, and finally washed with PBS for 3 min. The slides were then incubated in goat anti-chicken antibody (Alexa Fluor 488, 1:400; Life Technologies) and Alexa Fluor 568 Phalloidin (1:400; Life Technologies) for 30 min. Slides were then washed with PBS containing 0.05% Tween 20 twice for 3 min and finally washed with PBS for 3 min. The cover slips were mounted using Prolong Diamond (Thermo Fischer Scientific). Three-dimensional structured illumination microscopy (SIM) was carried out with a Nikon Structured Illumination Super-Resolution Microscope System (Nikon N-SIM; Nikon, Tokyo, Japan) using an oil immersion objective lens CFI SR (Apochromat TIRF100×, 1.49 NA; Nikon).

Statistical analysis

Because measurements of cell stiffness are not normally distributed (11,12,30,31), data were logarithmically transformed for statistical analysis and determined as geometric means ± standard error around the geometric mean (15) for each cell strain, unless otherwise indicated; averages taken over cell strains were arithmetic. Statistical significance of the effect of drug concentration (dexamethasone) on log cell stiffness or log cell traction was examined using linear regression. Analysis of variance was used to compare the effects of inductions of GFP, α-actinin, or RhoA on log cell stiffness and to compare vimentin-KO MEFs with controls, allowing for unequal variance between groups and using Tukey to account for multiple comparisons. JMP was used for these analyses with a significance level of 0.05; the minimal reported p-value is 10^{-4}. Details of which JMP routines were used are found in the Supporting Materials and Methods.

FEM

Finite-element modeling (FEM) was used to model the influence of the cell cortex on AFM and OMTC measurements of cell modulus, following the approaches of Vargas-Pinto et al. (12) and Mijailovich et al. (32), respectively. The cell was modeled as a cylinder of radius 10 μm (AFM) or 22.5 μm (OMTC) and a range of cell thickness from 2.75 to 15 μm, with a nominal thickness of 5 μm. The radius of the cell was chosen to be sufficiently large such that the strains at the edge of the domain were less than 0.1% of the maximal strain near the probes, and a 50% increase in radius did not significantly affect the results (<0.1% difference in all parameters for AFM and <0.13% for OMTC). Except for very small or narrow cells, the assumed shape of the cells would therefore have little effect on the results.

The cortex of the cell was on its upper surface and had a thickness of 400 nm (12) in all cases, with no slip between the cortex and internal cytoskeleton (32); we have previously examined the effect of variations in cortex thickness and found that the modeling results are not particularly sensitive to this parameter (12). The intracellular cytoskeleton and cortex are each modeled as homogeneous elastic materials, with the cortex having a modulus that ranged from 1 to 100 times the modulus of the intracellular cytoskeleton. Although the material was assumed to be incompressible, a Poisson's ratio of 0.49 was used for numerical stability. The AFM round tips and OMTC probes were modeled as rigid spheres (12,32). The bottom surface of the cell for both AFM and OMTC was pinned for zero displacement; the other surfaces were stress free except where the probes contacted the cell, as discussed below. Stress, strain, and deformation fields were determined using ABAQUS/CAE 6.13 finite-element software (Simulia, Providence, RI) with an explicit solver (33). An apparent modulus ($E_{apparent}$) of an equivalent single-layer, homogeneous cell was computed that would deform to the same extent as the two-layer cell model for the same external torque (OMTC) or force (AFM).

Model of AFM tip

A two-dimensional axisymmetric model was used (12). The indentation is assumed to be frictionless, consistent with the Hertz model (12), and the apical surface of the cortex was assumed to remain in contact with the AFM tip throughout the deformation process (34). The diameter of AFM rounded probes investigated varied from 0.8 to 10 μm and had an indentation into the cell of 400 nm. For the AFM sharp tip, a conical shape was assumed with a tip radius of 20 nm and a tip half angle of $\theta = 20°$. Indentation of the sharp tip into the cell was limited to 80 nm because higher indentations caused excessive numerical element distortion, and even with remeshing, the model did not converge to a solution, a limitation noted

Please cite this article in press as: Vahabikashi et al., Probe Sensitivity to Cortical versus Intracellular Cytoskeletal Network Stiffness, Biophysical Journal (2019), https://doi.org/10.1016/j.bpj.2018.12.021

in other such studies (12,35). This is also the reason that round-tip probes smaller than 0.8 μm in diameter could not be modeled for a 400 nm indentation. We note that the behavior for progressively smaller round tips, indenting 400 nm into a cell, are consistent with our results for a sharp tip indented 80 nm into a cell (e.g., Figs. 6, S4, and S5). Nonetheless, it is a limitation of this study that we were not able to model sharp-tip indentations greater than 80 nm.

To calculate $E_{apparent}$ for AFM, the reaction force for the given indentation of the AFM tip into the cell were determined using ABAQUS for each case and matched to that of a homogenous case (cortex and internal cytoskeleton with equal modulus) that gave the same force for the same indentation.

OMTC model

For OMTC modeling, a full three-dimensional geometry model was used. A no-slip boundary condition was applied between the probe (4.5 μm in diameter) and cell cortex (32). The magnetic field applied in OMTC was modeled as a torque per unit volume (60 Pa (32)) applied to the center of the bead, causing the bead to rotate around its central axis. Depth of the bead embedding was varied from 10 to 50% of the bead diameter (36,37). To calculate $E_{apparent}$ for each case, the horizontal displacement of the OMTC probe for the given torque was determined using ABAQUS and matched to that of a homogenous case (cortex and cytoskeleton with same modulus) that had the same torque. To validate our model, we followed Mijailovich et al. (32,33) and defined a parameter β that allowed an effective shear modulus ($G_d = \beta G$) to be determined based on bead-embedding depth:

$$\beta = \left(\frac{T_s R}{6 d}\right) \Big/ G,$$

where T_s is the torque applied per unit bead volume, R is the bead radius, d is the bead linear translation caused by the applied torque, and G is the shear modulus of the homogenous medium in which the bead is embedded. β can be thought of as the effective stiffness of the cell (torque required for a given bead rotation) at a given bead-embedding depth relative to the stiffness that would be seen for a homogenous cell with $E_{cortex} = E_{intracellular}$ and a bead-embedding depth of 50% in an infinite medium. We found values of β that were in good agreement with those found by Mijailovich et al. for the case they examined ($E_{cortex} = E_{intracellular}$) (see Fig. S10).

RESULTS

Alterations induced by dexamethasone, α-actinin, and RhoA

The monolayer of endothelial cells lining the inner wall of SC in the eye is subject to a pressure gradient, and the mechanical properties of these cells have been shown to be important to their biological barrier function (15). Using AFM, TM, and OMTC, here we further characterized the mechanical properties of these cells before and after treatment with dexamethasone or transduction with adenovirus encoding for RhoA or α-actinin. Dexamethasone can cause glaucoma and is known to generate cytoskeletal changes in SC cells (38); RhoA is a cytoskeletal regulator (39), and α-actinin is an actin cross-linker (40).

Figs. 1 and S11 shows the distribution of filamentous actin (F-actin) and phosphorylated myosin light chain (p-myosin) in confluent SC cells treated with dexamethasone (1 μM) as compared with controls. In both control and treated cells, we found stress fibers distributed throughout the cells, particularly along the cell peripheries (Fig. 1, *A* and *D*). The distribution of p-myosin was similar to that of F-actin (Fig. 1, *B* and *E*). Compared to control treatment, we found that dexamethasone-treated cells had denser stress fibers and p-myosin at the periphery of the cells. Fluorescent intensity measurements confirmed these conclusions, showing that the dexamethasone-treated group (1 μM) had higher cortical F-actin ($p < 10^{-4}$) and p-myosin ($p = 0.0002$) as compared with control.

Increasing concentrations of dexamethasone caused dosage-dependent increases in both SC cell stiffness (with sharp-tip AFM) and cell traction (TM), respectively (Fig. 2 *A*; linear regression: $p < 10^{-4}$). In contrast, dexamethasone had either no effect on SC cell stiffness as measured with AFM round tips ($p \approx 1$) or a small statistically significant decrease in cell stiffness as measured with OMTC (Fig. 2 *B*; $p < 10^{-4}$).

Fig. 3 shows the distribution of F-actin in SC cells before and after transduction with green fluorescent protein (GFP: a control) or overexpression with α-actinin or RhoA. Cells in the GFP group (Fig. 3 *B*) had an F-actin distribution similar to that of control cells (Fig. 3 *A*). However, cells transduced with either α-actinin or RhoA showed an altered morphology with thicker and more prominent cortical stress fibers (*arrows* in Fig. 3, C and *D*).

Comparison of cell stiffness in WT and GFP-transduced cells using AFM with a sharp tip showed no difference ($p > 0.8$). However, overexpression of both α-actinin ($p < 10^{-4}$) and RhoA ($p < 10^{-4}$) increased cell stiffness compared to control cells or cells transduced with GFP (Fig. 2 *C*). Using TM, we found traction to be increased after transduction of RhoA ($p < 10^{-4}$) compared to GFP-transduced cells and controls (Fig. 2 *C*). Because of one nonresponsive cell strain (Fig. S3 *C*), the increased traction after transduction of α-actinin was not statistically significant ($p > 0.3$). In contrast, measurements with both AFM round tips and OMTC showed that overexpression of α-actinin and RhoA decreased cell stiffness compared with control cells (AFM: $p < 0.03$; OMTC: $p < 10^{-4}$) (Fig. 2 *D*). When compared with the GFP group, AFM round tips revealed a trend for decreased cell stiffness for the α-actinin and RhoA overexpression groups, whereas OMTC revealed a trend for increased cell stiffness, but in neither case was the difference significant (Fig. 2 *D*). OMTC also showed that GFP decreased cell stiffness relative to control cells ($p < 0.001$); this trend was also apparent with AFM round tips but was not statistically significant ($p > 0.4$).

Vimentin KO reduces cell stiffness and traction

Vimentin is a type III intermediate filament protein that assembles into a major cytoskeletal system (41–43). To study the role of vimentin in cytoskeletal mechanics, we used immortalized MEFs isolated from a mouse KO of

Please cite this article in press as: Vahabikashi et al., Probe Sensitivity to Cortical versus Intracellular Cytoskeletal Network Stiffness, Biophysical Journal (2019), https://doi.org/10.1016/j.bpj.2018.12.021

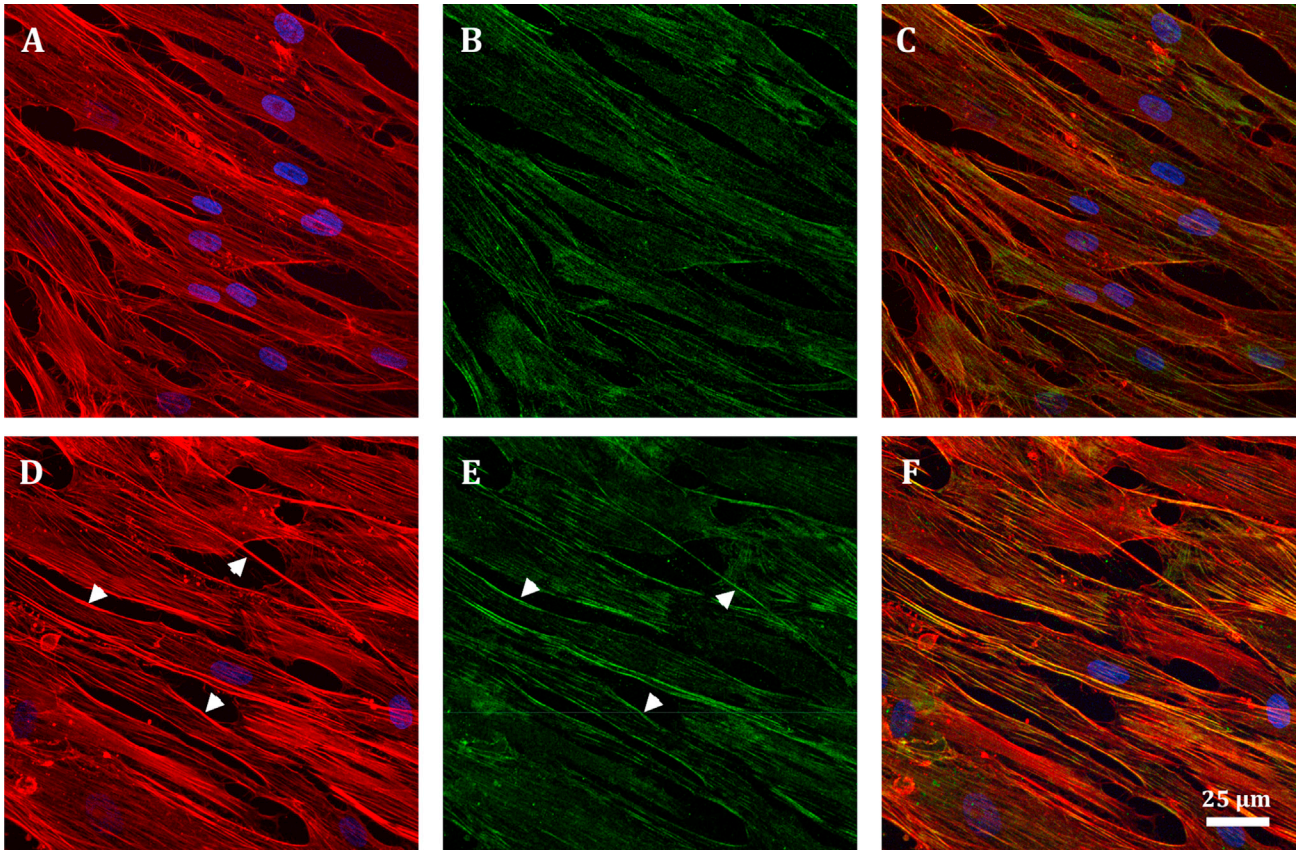

FIGURE 1 Confocal images of confluent monolayer of vehicle-only control (*top row*) as compared with 1-μM-dexamethasone-treated (*bottom row*) SC cells; F-actin (*red*) (*A* and *D*), phosphorylated myosin (*green*) (*B* and *E*), nucleus (*blue*). Cortex and stress fibers are seen in both groups, but the cortex is more prominent in treated SC cells (*white arrows* in (*D*)). Also, although p-myosin is present in both groups, it is more concentrated at the cortex of treated cells (*white arrows* in (*E*)). (*C*) and (*F*) are overlaid images.

the intermediate filament gene encoding vimentin (19). In vimentin-KO MEFs, there was no vimentin, as expected, and in WT MEFs, there was a robust network of vimentin intermediate filaments throughout the cell body (Fig. 4, *C* and *D*). In WT cells, vimentin filaments were mostly found in the intracellular region but also within close proximity to the actin-rich cortex (Fig. 4, *E–G*). No obvious difference was seen in the F-actin distribution between the WT and vimentin-KO MEFs (Fig. 4, *A* and *B*).

We compared the mechanical behavior of vimentin-KO MEFs to WT MEFs using both confluent and sparsely confluent seeding conditions. Vimentin-KO MEFs were generally softer than WT MEFs (using AFM sharp tips: confluent monolayers, $p < 0.03$, Fig. 2 *E*; sparsely cultured, $p < 0.01$, Fig. 2 *G*) and exerted less traction (using TM: confluent monolayers, $p < 0.03$, Fig. 2 *E*; sparsely cultured, $p < 0.01$, Fig. 2 *G*). Using AFM round tips, we also found that vimentin-KO MEFs were softer than WT MEFs, but the differences did not reach statistical significance for either confluent monolayers ($p < 0.3$) or sparsely cultured cells ($p < 0.07$) (Fig. 2, *F* and *H*).

Unexpectedly, when we measured stiffness using OMTC, the vimentin-KO MEFs were stiffer than WT MEFs (confluent monolayers, $p < 0.0001$; sparsely cultured cells, $p < 0.02$) (Fig. 2, *F* and *H*). These observations were in contrast to the measurements taken using AFM sharp tips, AFM round tips, and TM. To understand why the results obtained by OMTC differed from those obtained by AFM and TM in MEFs, we measured the bead-embedding depth and cell thicknesses, both of which impact stiffness measured by OMTC (32). We found that the bead-embedding depth was similar in both cell types, with no significant difference between WT and vimentin-KO MEFs (mean of 63%, $n = 14–18$; $p > 0.6$). However, the thickness of the vimentin-KO MEFs (3.2 ± 0.4 μm, mean ± SD; $n = 20$) was significantly smaller than that of the WT MEFs (4.2 ± 0.5 μm, mean ± SD; $n = 30$) (Fig. 5) ($p < 10^{-4}$). As shown below, FEM reconciles these observations.

FEM shows that the cell cortex differentially affects differing measurements of cell stiffness

To model OMTC, we followed the approach of Mijailovich et al. (32) but allowed for a cell cortex that was significantly stiffer than the underlying intracellular network. To model AFM, we extended the approach of Vargas-Pinto et al.

Please cite this article in press as: Vahabikashi et al., Probe Sensitivity to Cortical versus Intracellular Cytoskeletal Network Stiffness, Biophysical Journal (2019), https://doi.org/10.1016/j.bpj.2018.12.021

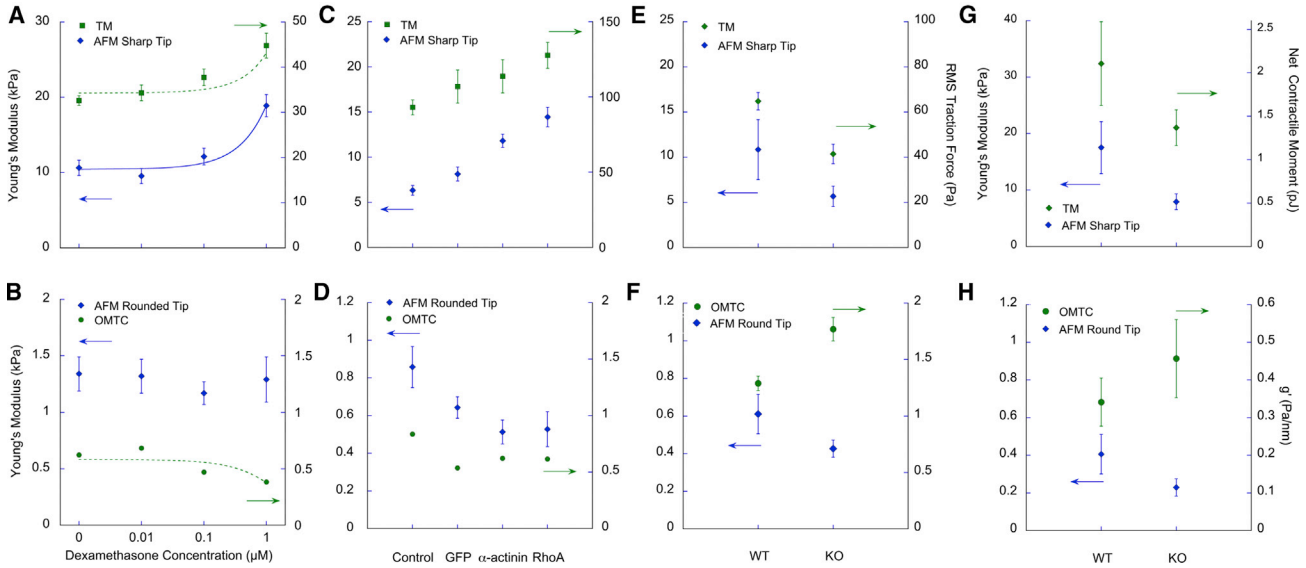

FIGURE 2 Measurements of cell biophysical properties of SC cells after (*A* and *B*) treatment with varying concentrations of dexamethasone as compared with vehicle alone or (*C* and *D*) overexpression of α-actinin or RhoA as compared with GFP or control. (*E*)–(*H*) show comparison of wild-type (WT) MEFs with vimentin KO. Superconfluent monolayers were used for the dexamethasone studies on SC cells (*A* and *B*), confluent for the α-actinin or RhoA expression studies on SC cells (*C* and *D*), and both confluent (*E* and *F*) and sparsely seeded (*G* and *H*) cells for the MEF studies, as described in the Materials and Methods. Geometric mean ± standard error about geometric means is shown. Curves shown in (*A*) and (*B*) are best regression fits to the data; the equations are given in Supporting Materials and Methods. Data for individual cell strains are found in Figs. S2 and S3. To see this figure in color, go online.

(12) to determine the effect of AFM tip size. We modeled a cell as a thin cylinder with a nominal thickness of 5 μm that had two layers: a 400 nm thick cortex and an underlying intracellular network. Embedded in the top of the cell was either a sharp or round AFM tip that exerted a vertical force on the cell or a round OMTC probe that exerted a torque on the cell. Details are in the Materials and Methods.

We first examined the strain-energy density distribution caused by AFM tips or the OMTC probe when the cortex has the same stiffness (E_{cortex}) as the intracellular cytoskeleton ($E_{intracellular}$) and when it is 50 times stiffer (Fig. 6; Supporting Materials and Methods). For the AFM sharp tip, strain energy is largely confined to the cortex (Fig. 6, *A* and *B*), consistent with the previous findings (12). For the smallest AFM round-tip probe (0.8 μm), strain energy is also largely confined to the cortex but extends appreciably into the intracellular network as well, particular for the case of a stiff cortex (Fig. 6, *C* and *D*). For the largest AFM round-tip probe (10 μm), strain energy extends throughout the cell beneath the probe but is somewhat broader for the case of a stiff cortex (Fig. 6, *E* and *F*). Finally, for OMTC, the strain-energy distribution is intermediate between the cases of the small and larger AFM tips but is more similar to the latter, with the strain energy spread out more broadly for the case of a stiff cortex (Fig. 6, *G* and *H*).

These results suggest that when the size of probe exceeds the thickness of cortex, strain energy spreads out of the cortex, particularly when the cortex is much stiffer than the intracellular network.

The effect of cortex stiffness on measurements by AFM and OMTC was quantified by computing an apparent modulus ($E_{apparent}$) for an equivalent single-layer, homogeneous cell that deformed to the same extent as the cell model with cortex as a function of $E_{cortex}/E_{intracelluar}$ (see Materials and Methods). For AFM sharp tips, $E_{apparent}$ ranged from 65 to 100% of E_{cortex} (Fig. 7 *A*, *inset*), whereas for AFM round tips, $E_{apparent}$ was less than 10% of E_{cortex}. For an AFM tip diameter of 10 μm, $E_{apparent}$ was nearly independent of E_{cortex} and near the value of $E_{intracelluar}$ (Fig. 7 *A*).

For OMTC, the predictions were similar to those of AFM round tips, with $E_{apparent}$ much closer to $E_{intracelluar}$ than to E_{cortex} (Fig. 7 *B*). These results were very different than those of AFM sharp tips and show that the stiffness measured by OMTC is largely characteristic of the intracellular network, although it is still somewhat affected by cortex stiffness. Interestingly, embedding depth does not have a monotonic effect on $E_{apparent}$ but decreases with embedding depth for shallow embedding and then reversing this trend for deeper embedding (Figs. 7 *B* and S7). This is caused by the distal cortex (the cortex that is not surrounding the bead) that becomes somewhat more important for deeply embedded beads (Fig. S8), and by a substrate effect (insert in Fig. 7 *B*; Supporting Materials and Methods).

The effect of decreased KO MEF cell thickness on OMTC and AFM measurements

Our OMTC measurements suggested that vimentin-KO MEFs were stiffer than WT MEFs, in contrast with the

Please cite this article in press as: Vahabikashi et al., Probe Sensitivity to Cortical versus Intracellular Cytoskeletal Network Stiffness, Biophysical Journal (2019), https://doi.org/10.1016/j.bpj.2018.12.021

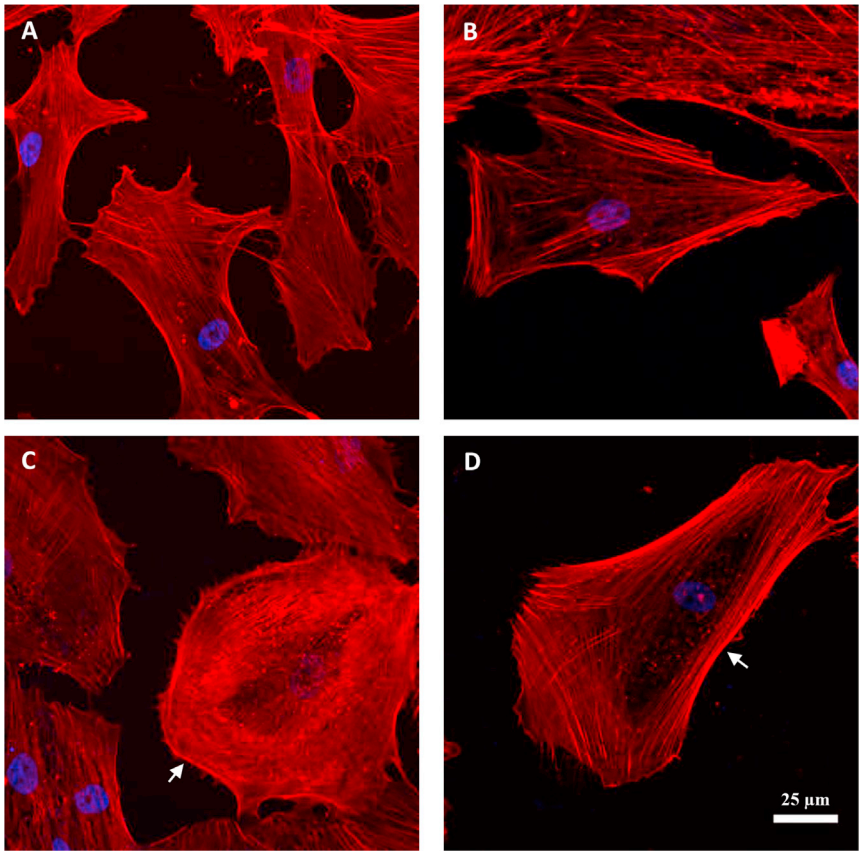

FIGURE 3 Confocal images of SC cells. (*A*) WT-non-transduced, (*B*) GFP-transduced, (*C*) α-actinin-transduced, and (*D*) RhoA-transduced cells are shown; F-actin (*red*), nucleus (*blue*). Control and GFP groups had similar F-actin distribution and cortex structure (*A* and *B*). The α-actinin-transduced cells showed an altered morphology and had a relatively thicker cortex (*white arrow* in (*C*)). The RhoA-transduced cells showed significant accumulation of stress fibers at peripheral regions and a more prominent cortex (*white arrow* in (*D*)).

measurements using the other techniques (Fig. 2, *E–H*). Because we found that vimentin-KO MEFs are thinner than WT MEF, we examined whether this thickness difference might explain the discrepancy, particularly in the context of deeply embedded OMTC beads. For cells thinner than 5 μm, the modulus rises rapidly with decreasing cell thickness (*inset*, Fig. 7 *B*; Fig. S6), which is a behavior that would explain why the OMTC showed KO MEFs to be stiffer than WT. The effect of decreased thickness of KO MEFs on $E_{apparent}$ (Fig. S9) would also explain why the AFM round-tip results were lower in KOs than WTs but did not reach statistical significance.

DISCUSSION

Here, we have examined how the choice of surface probe impacts the measurement and interpretation of cell biomechanical properties. In response to a panel of interventions and in both cell types investigated, cell stiffness measured using AFM sharp tips and contractile forces measured using TM tracked similarly to one another (Fig. 2, *A* and *C*). However, these measures did not track with cell stiffness measured by OMTC or with AFM round tips. To explain these differential responses, we turned to FEM simulations. Simulations of AFM round tips (5 μm or larger) and OMTC were sensitive to stiffness of the intracellular network but relatively insensitive to stiffness of the cell cortex (Fig. 7, *A* and *B*); these results also showed that OMTC is particularly sensitive to cell thickness. Simulations of AFM sharp tips, by contrast, were more sensitive to the stiffness of the cell cortex, with values of $E_{apparent}$ comparable to cortex stiffness (Fig. 7 *A*, *inset*). Taken together, these findings suggest that measurements using AFM sharp tips and TM tend to emphasize biomechanical properties of the cell cortex, whereas measurements using OMTC and AFM round tips tend to emphasize stiffness of the intracellular network.

OMTC measurements on cells previously have been suggested to characterize cortical stiffness (11,18,28,44). The relative insensitivities of OMTC to cortex stiffness found in our simulations were due to the large size of these probes as compared to the thickness of the cortex, leading to substantial strain energy in the intracellular network. Our finding that OMTC is sensitive to intracellular network stiffness is consistent with studies of molecular crowding caused by cellular volume reduction, showing increased cell stiffness as measured using OMTC but no change in cellular contractile force as measured by TM (23,28).

We note that the FEM used here greatly simplifies cytoskeletal mechanics by treating the cortical and intracellular networks as two homogeneous, linearly elastic materials. The goal of these models was not to replicate the complex geometry of the cytoskeleton but instead to evaluate how

Please cite this article in press as: Vahabikashi et al., Probe Sensitivity to Cortical versus Intracellular Cytoskeletal Network Stiffness, Biophysical Journal (2019), https://doi.org/10.1016/j.bpj.2018.12.021

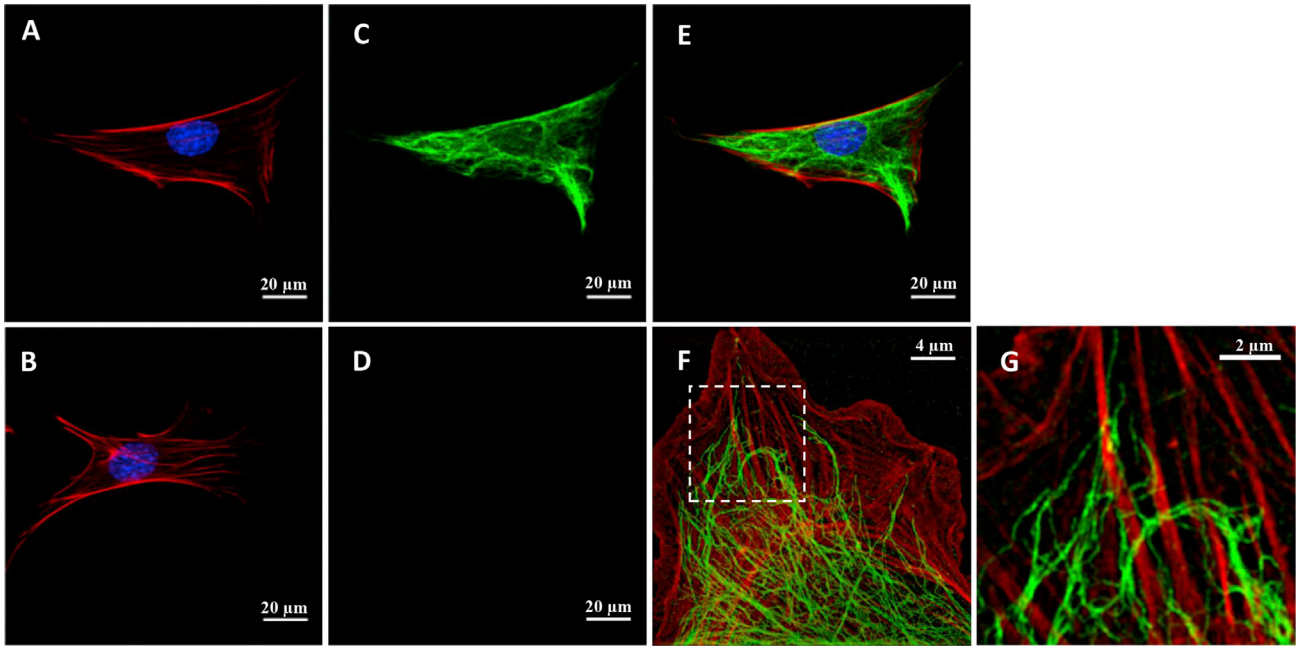

FIGURE 4 Confocal images showing F-actin (*red*), nucleus (*blue*) (*A* and *B*), and vimentin intermediate filaments (*green*) (*C* and *D*) of WT MEFs (*A* and *C*) and vimentin-KO MEFs (*B* and *D*). (*D*) shows no staining in a vimentin-KO MEF. (*E*) shows a merged image of (*A*) and (*B*). (*F*) is a structured illumination micrograph (SIM) of a WT MEF at the basal cortex level, showing the close association between actin stress fibers and vimentin intermediate filaments. A magnified image of the inset in (*F*) showing vimentin intermediate filaments surrounding and interconnecting actin stress fibers is given (*G*).

a stiff cortex may affect measurements of cell stiffness using different probes. Because these measurements are conventionally interpreted using models of cells that are homogeneous and linearly elastic (21,32,45,46), examining the effect of a stiff cortex on these stiffness measurements necessarily required use of a similar model, modified to include a cortex. A more realistic FEM model of the cell would likely further strengthen our conclusions because the intracellular cytoskeletal network is connected to the cortical network, and this will induce propagation of apically applied force or torque from OMTC beads or larger AFM rounded probes to deeper cytoskeletal structures or even basal regions of the cell (47,48).

Vimentin is a structural protein that polymerizes into a major intermediate filament cytoskeletal system (27,41,49,50). Our imaging studies showed a network of vimentin intermediate filaments in WT MEFs that were entirely absent in vimentin-KO MEFs (Fig. 4, *C* and *D*). We also saw evidence of vimentin in the actin-rich cortical region of the WT MEFs (Fig. 4, *F* and *G*), in agreement with previous findings in chicken embryonic fibroblasts (51) and bovine pulmonary artery endothelial cells (52). We used AFM sharp tip and TM to measure cell stiffness and contractile state of the cortex of the cells and found both significantly reduced in vimentin-KO MEFs as compared to WT MEFs (Fig. 2, *E* and *G*), leading us to conclude that vimentin intermediate filaments contribute to or influence cortical stiffness and cellular contractile force. Measurements using AFM round tips allowed us to conclude that the intracellular network of vimentin-KO MEFs also has reduced stiffness as compared to WT MEFs (Fig. 2, *F* and *H*).

Guo et al. (18) used optical tweezers and found that the cytoplasmic stiffness of vimentin-KO MEFs was reduced as compared to WT MEFs, consistent with our finding of reduced intracellular stiffness. They also used OMTC and concluded that vimentin does not influence cortical stiffness, in contrast to our AFM sharp-tip and TM findings. However, we found decreased thickness in vimentin-KO MEFs relative to WT MEFs (Fig. 5), consistent with a previous report (53), and were able to show that these cell thickness differences would substantially impact OMTC measurements of cell stiffness (Fig. 7 *B*, *inset*). Thus, OMTC measurements of vimentin-KO MEFs' stiffness may not be reflective of the cells' intrinsic mechanics.

Wang and Stamenović (54) found that at low levels of strain, the stiffness of WT and vimentin-KO MEFs as measured using OMTC were similar to one another, whereas at higher strain levels, the stiffness of WT cells

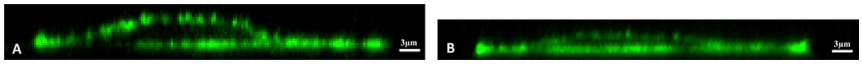

FIGURE 5 Confocal cross-sectional representative images of typical WT (*A*) and vimentin-KO (*B*) MEFs show that the vimentin-KO MEFs are thinner than the WT MEFs.

Please cite this article in press as: Vahabikashi et al., Probe Sensitivity to Cortical versus Intracellular Cytoskeletal Network Stiffness, Biophysical Journal (2019), https://doi.org/10.1016/j.bpj.2018.12.021

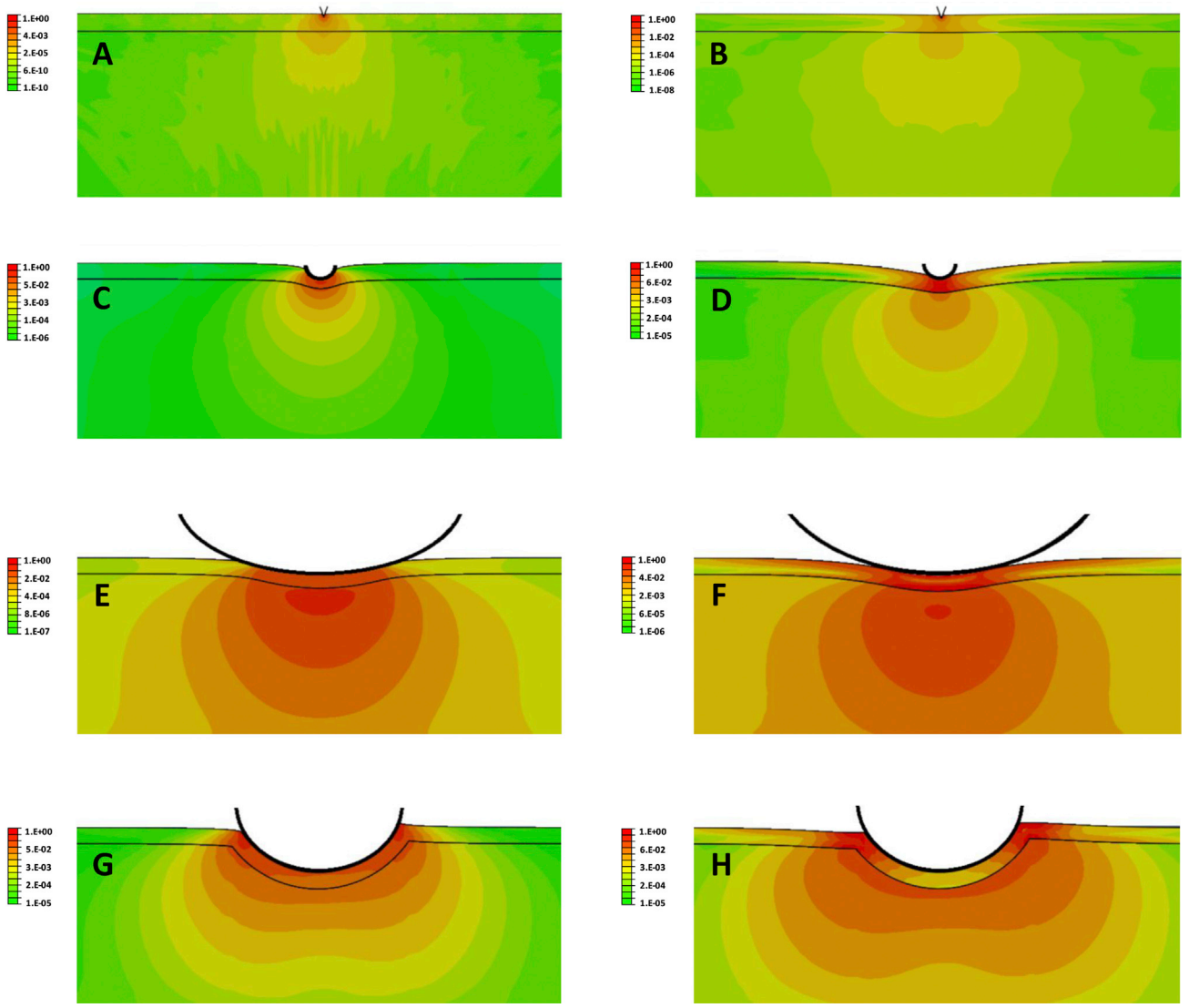

FIGURE 6 Strain-energy distribution (log scale) for indentation into a cell of a sharp AFM tip (*A* and *B*), a 0.8 μm diameter rounded AFM tip (*C* and *D*), a 10 μm diameter rounded AFM tip (*E* and *F*), and a 4.5 μm OMTC bead (*G* and *H*). The indentation is smaller in cases (*A*) and (*B*) (80 nm) because of numerical limitations, as discussed in the Materials and Methods, than for the other AFM tips (400 nm). The OMTC bead is embedded 25% of its diameter into the cell and twisted by a torque of 60 Pa applied in a counterclockwise fashion. (*A*), (*C*), (*E*), and (*G*) are for cases with $E_{cortex} = E_{intracellular}$; (*B*), (*D*), (*F*), and (*H*) are for $E_{cortex} = 50 \times E_{intracellular}$. The cortex in each panel is the narrow region between the two horizontal black lines and has a thickness of 400 nm before indentation. The strain-energy distribution in each panel is normalized to the maximal strain energy in that panel, and a log scale is used. Cell thickness is 5 μm.

was greater than that of vimentin-KO cells. Mendez et al. reported similar results using AFM round tips (55), and these investigators concluded that the vimentin network contributes to cell stiffness when the cytoskeleton is under high levels of strain. Our studies are consistent with this finding, showing that WT cells had a higher cell stiffness than vimentin-KO cells when measured with sharp AFM tips that generate high levels of strain as compared with AFM round tips and OMTC that generate much lower levels of strain (Figs. 2 and S4).

Our studies focused on examining regional differences in cytoskeletal structure and how these differences affect measurements of cell mechanics by external probes. We examined the effect of several agents that were anticipated to affect cellular mechanics and found that they affected the cortical regions differently than the intracellular network. RhoA regulates cytokinesis (3), causing stiffening of the cell cortex (3) and retraction of the vimentin intermediate filament network (56–58). This is consistent with our findings that RhoA overexpression increases cortical cell stiffness and traction as measured by AFM sharp tips and TM, respectively, and somewhat reduces intracellular network cell stiffness as measured by AFM round tips (see Fig. 2). This may also relate to our finding that α-actinin

Please cite this article in press as: Vahabikashi et al., Probe Sensitivity to Cortical versus Intracellular Cytoskeletal Network Stiffness, Biophysical Journal (2019), https://doi.org/10.1016/j.bpj.2018.12.021

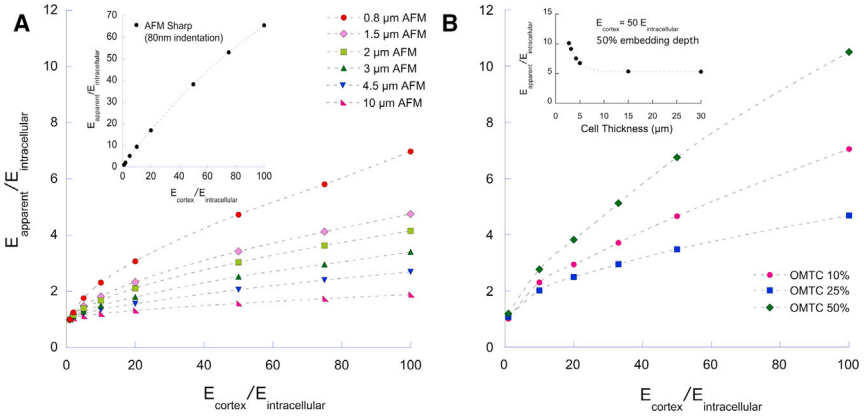

FIGURE 7 (*A*) $E_{apparent}/E_{intracellular}$ as a function of $E_{cortex}/E_{intracellular}$ for an AFM round tip of diameter 0.8–10 μm with an indentation of 400 nm. Inset shows result for AFM sharp tip with indentation of 80 nm. Cell thickness is 5 μm. (*B*) $E_{apparent}/E_{intracellular}$ as a function of $E_{cortex}/E_{intracellular}$ for an OMTC probe of diameter 4.5 μm for embedding depths of 10, 25, or 50% of bead diameter is shown. Cell thickness is 5 μm. Inset shows results for an OMTC probe embedded 50% into a cell with $E_{cortex}/E_{intracellular} = 50$ for cell thicknesses ranging from 2.75 to 30 μm. To see this figure in color, go online.

overexpression causes similar changes (59,60). These results also show that overexpression of regulatory factors such as RhoA and α-actinin can be transduced into cells to alter their cortical stiffness.

We also found that dexamethasone caused an increase in the cortical stiffness of SC cells (Fig. 2 *A*), along with increased density of cortical F-actin and p-myosin (Fig. 1) with little effect on the intracellular network (Fig. 2 *B*). Dexamethasone induces RhoA activation (61) and is associated with elevated stress fiber formation in human trabecular meshwork cells (62,63), decreased hydraulic conductivity of SC and trabecular meshwork cell monolayers (64), and increased traction in alveolar epithelial cells (65). This may be related to the vasoconstriction that steroids are known to promote (66). Corticosteroids such as dexamethasone are widely used to offset allergies, asthma, and skin rashes, but their ocular use is known to elevate intraocular pressure in some individuals and can cause glaucoma (67). Our studies here, when considered with our previous work showing glaucomatous SC cells to have increased stiffness (15), provide a mechanism by which dexamethasone could cause the elevated intraocular pressure characteristic of glaucoma.

Our AFM measurements, combined with FEM, suggest that the stiffness of the intracellular network is roughly 0.25–1 kPa (Figs. 2, *B*, *D*, *F*, and *H* and 7 *A*), whereas that of the cortical cytoskeleton is at least one order of magnitude higher (Figs. 2, *A*, *C*, *E*, and *G* and 7 *A*, *inset*). As expected, both values are much higher than the reported stiffness of cytoplasm (0.005–0.01 kPa) measured using optical tweezers (18), and thus no conclusions can be drawn from our studies with respect to the cytoplasm (11). Table 1 shows a summary of our findings regarding the behavior of the different measurement techniques on the cells considered in this study. A recent report by Wu et al. (68) using MCF-7 cells is consistent with these findings.

Our studies show that measurements of cell mechanics by different external probes are differentially sensitive to regional differences in cytoskeletal structure. Although stiffnesses measured by AFM sharp tips characterize the stiff cortical region of the cells, which is under active traction, similar trends are observed in cellular contractile force measurements by TM; this suggests that cells modulate both cortical stiffness and traction force through a similar mechanism. In contrast, AFM round tips and OMTC are both less influenced by the cortex and instead probe the stiffness of the noncortical intracellular network. These interpretations are supported by our FEM studies, which also demonstrate that probe sensitivity to cell thickness can explain the OMTC trends. By considering the regional emphasis of each probe type, our results additionally show that vimentin intermediate filaments play significant mechanical roles in both the intracellular and cortical domains of cells. Taken together, these results highlight the importance of probe choice in the interpretation of cellular mechanics measurements.

SUPPORTING MATERIAL

Supporting Materials and Methods and 11 figures are available at http://www.biophysj.org/biophysj/supplemental/S0006-3495(19)30018-9.

TABLE 1 Summary of Findings from Experimental Measurements and FEM

Technique	Typical Modulus^{+}/Stress*	Measurement Locus	Sensitivity to Cell Thickness
AFM sharp tip	5–20 kPa^{+}	cortical	insensitive
AFM 1.5 μm rounded tip	0.5–4 kPa^{+}	cortical and intracellular	relatively insensitive
AFM 10 μm rounded tip	0.25–1.5 kPa^{+}	intracellular network	sensitive
OMTC	0.5–2 kPa^{+}	cortical and intracellular	sensitive
TM	0.02–0.5 kPa*	cortical	not investigated

Please cite this article in press as: Vahabikashi et al., Probe Sensitivity to Cortical versus Intracellular Cytoskeletal Network Stiffness, Biophysical Journal (2019), https://doi.org/10.1016/j.bpj.2018.12.021

AUTHOR CONTRIBUTIONS

A.V., M.J., C.Y.P, K.P., W.D.S., and C.Y.P. designed the experiments. A.V., C.Y.P., Z.Z., E.K.D., and H.W. performed the experiments. A.V., M.J., C.Y.P., J.J.F., and D.A.W. designed and evaluated the model. A.V. implemented the model and performed the simulations. K.P., W.D.S., and R.D.G. supplied the cell lines. A.V., M.J., C.Y.P., J.J.F., R.D.G., K.P., W.D.S., D.A.W., and H.W. analyzed the data and wrote the manuscript.

ACKNOWLEDGMENTS

We acknowledge support from National Institutes of Health EY019696 (M.J., W.D.S., and J.J.F.), P01HL120839 (J.J.F. and D.A.W.), P01GM096971 (R.D.G., D.A.W.), and U54 CA193419 (R.D.G.), Northwestern University Atomic and Nanoscale Characterization Experimental Center Center, Center for Advanced Molecular Imaging, and the National Natural Science Foundation of China (11472062, Z.Z.).

REFERENCES

1. Wang, J., X. Liu, and Y. Zhong. 2013. Rho/Rho-associated kinase pathway in glaucoma (Review). *Int. J. Oncol.* 43:1357–1367.
2. Wang, S. K., and R. T. Chang. 2014. An emerging treatment option for glaucoma: Rho kinase inhibitors. *Clin. Ophthalmol.* 8:883–890.
3. Chircop, M. 2014. Rho GTPases as regulators of mitosis and cytokinesis in mammalian cells. *Small GTPases.* 5:e29770.
4. Lecuit, T., and P. F. Lenne. 2007. Cell surface mechanics and the control of cell shape, tissue patterns and morphogenesis. *Nat. Rev. Mol. Cell Biol.* 8:633–644.
5. An, S. S., T. R. Bai, …, L. Wang. 2007. Airway smooth muscle dynamics: a common pathway of airway obstruction in asthma. *Eur. Respir. J.* 29:834–860.
6. Hoffman, B. D., and J. C. Crocker. 2009. Cell mechanics: dissecting the physical responses of cells to force. *Annu. Rev. Biomed. Eng.* 11:259–288.
7. Salbreux, G., G. Charras, and E. Paluch. 2012. Actin cortex mechanics and cellular morphogenesis. *Trends Cell Biol.* 22:536–545.
8. Agus, D. B., J. F. Alexander, …, P. H. Wu; Physical Sciences - Oncology Centers Network. 2013. A physical sciences network characterization of non-tumorigenic and metastatic cells. *Sci. Rep.* 3:1449.
9. Stamer, W. D., S. T. Braakman, …, M. Johnson. 2015. Biomechanics of Schlemm's canal endothelium and intraocular pressure reduction. *Prog. Retin. Eye Res.* 44:86–98.
10. Ratz, P. H. 2011. Mechanics of vascular smooth muscle. *Compr. Physiol.* 6:111–168.
11. Hoffman, B. D., G. Massiera, …, J. C. Crocker. 2006. The consensus mechanics of cultured mammalian cells. *Proc. Natl. Acad. Sci. USA.* 103:10259–10264.
12. Vargas-Pinto, R., H. Gong, …, M. Johnson. 2013. The effect of the endothelial cell cortex on atomic force microscopy measurements. *Biophys. J.* 105:300–309.
13. Guo, M., A. J. Ehrlicher, …, D. A. Weitz. 2014. Probing the stochastic, motor-driven properties of the cytoplasm using force spectrum microscopy. *Cell.* 158:822–832.
14. Zhou, E. H., R. Krishnan, …, M. Johnson. 2012. Mechanical responsiveness of the endothelial cell of Schlemm's canal: scope, variability and its potential role in controlling aqueous humour outflow. *J. R. Soc. Interface.* 9:1144–1155.
15. Overby, D. R., E. H. Zhou, …, M. Johnson. 2014. Altered mechanobiology of Schlemm's canal endothelial cells in glaucoma. *Proc. Natl. Acad. Sci. USA.* 111:13876–13881.
16. Fabry, B., G. N. Maksym, …, J. J. Fredberg. 2001. Selected contribution: time course and heterogeneity of contractile responses in cultured human airway smooth muscle cells. *J. Appl. Physiol.* 91:986–994.
17. Munevar, S., Y. Wang, and M. Dembo. 2001. Traction force microscopy of migrating normal and H-ras transformed 3T3 fibroblasts. *Biophys. J.* 80:1744–1757.
18. Guo, M., A. J. Ehrlicher, …, D. A. Weitz. 2013. The role of vimentin intermediate filaments in cortical and cytoplasmic mechanics. *Biophys. J.* 105:1562–1568.
19. Shabbir, S. H., M. M. Cleland, …, M. Mrksich. 2014. Geometric control of vimentin intermediate filaments. *Biomaterials.* 35:1359–1366.
20. Mao, W., T. Tovar-Vidales, …, A. F. Clark. 2011. Perfusion-cultured bovine anterior segments as an ex vivo model for studying glucocorticoid-induced ocular hypertension and glaucoma. *Invest. Ophthalmol. Vis. Sci.* 52:8068–8075.
21. Rico, F., P. Roca-Cusachs, …, D. Navajas. 2005. Probing mechanical properties of living cells by atomic force microscopy with blunted pyramidal cantilever tips. *Phys. Rev. E. Stat. Nonlin. Soft Matter Phys.* 72:021914.
22. Stamer, W. D., K. M. Perkumas, …, B. S. McKay. 2006. Coiled-coil targeting of myocilin to intracellular membranes. *Exp. Eye Res.* 83:1386–1395.
23. Zhou, E. H., X. Trepat, …, J. J. Fredberg. 2009. Universal behavior of the osmotically compressed cell and its analogy to the colloidal glass transition. *Proc. Natl. Acad. Sci. USA.* 106:10632–10637.
24. Park, C. Y., E. H. Zhou, …, R. Krishnan. 2015. High-throughput screening for modulators of cellular contractile force. *Integr. Biol (Camb).* 7:1318–1324.
25. Trepat, X., M. R. Wasserman, …, J. J. Fredberg. 2009. Physical forces during collective cell migration. *Nat. Phys.* 5:426–430.
26. Butler, J. P., I. M. Tolić-Nørrelykke, …, J. J. Fredberg. 2002. Traction fields, moments, and strain energy that cells exert on their surroundings. *Am. J. Physiol. Cell Physiol.* 282:C595–C605.
27. Mendez, M. G., S. Kojima, and R. D. Goldman. 2010. Vimentin induces changes in cell shape, motility, and adhesion during the epithelial to mesenchymal transition. *FASEB J.* 24:1838–1851.
28. Guo, M., A. F. Pegoraro, …, D. A. Weitz. 2017. Cell volume change through water efflux impacts cell stiffness and stem cell fate. *Proc. Natl. Acad. Sci. USA.* 114:E8618–E8627.
29. Laurent, V. M., S. Hénon, …, F. Gallet. 2002. Assessment of mechanical properties of adherent living cells by bead micromanipulation: comparison of magnetic twisting cytometry vs optical tweezers. *J. Biomech. Eng.* 124:408–421.
30. Park, C. Y., D. Tambe, …, J. J. Fredberg. 2010. Mapping the cytoskeletal prestress. *Am. J. Physiol. Cell Physiol.* 298:C1245–C1252.
31. Cai, P., Y. Mizutani, …, T. Okajima. 2013. Quantifying cell-to-cell variation in power-law rheology. *Biophys. J.* 105:1093–1102.
32. Mijailovich, S. M., M. Kojic, …, J. J. Fredberg. 2002. A finite element model of cell deformation during magnetic bead twisting. *J. Appl. Physiol.* 93:1429–1436.
33. Vahabikashi, A. 2017. Altered mechanics of Schlemm's canal endothelial cells and trabecular meshwork in glaucoma. Northwestern University, PhD thesis.
34. Harris, A. R., and G. T. Charras. 2011. Experimental validation of atomic force microscopy-based cell elasticity measurements. *Nanotechnology.* 22:345102.
35. Ng, L., H. H. Hung, …, A. Grodzinsky. 2007. Nanomechanical properties of individual chondrocytes and their developing growth factor-stimulated pericellular matrix. *J. Biomech.* 40:1011–1023.
36. Fabry, B., G. N. Maksym, …, J. J. Fredberg. 2001. Scaling the microrheology of living cells. *Phys. Rev. Lett.* 87:148102.
37. Zeng, D., T. Juzkiw, …, M. Johnson. 2010. Young's modulus of elasticity of Schlemm's canal endothelial cells. *Biomech. Model. Mechanobiol.* 9:19–33.
38. Clark, A. F., D. Brotchie, …, I. Grierson. 2005. Dexamethasone alters F-actin architecture and promotes cross-linked actin network formation in human trabecular meshwork tissue. *Cell Motil. Cytoskeleton.* 60:83–95.

39. Bustelo, X. R., V. Sauzeau, and I. M. Berenjeno. 2007. GTP-binding proteins of the Rho/Rac family: regulation, effectors and functions in vivo. *BioEssays.* 29:356–370.

40. Otey, C. A., and O. Carpen. 2004. Alpha-actinin revisited: a fresh look at an old player. *Cell Motil. Cytoskeleton.* 58:104–111.

41. Goldman, R. D., S. Khuon, …, P. M. Steinert. 1996. The function of intermediate filaments in cell shape and cytoskeletal integrity. *J. Cell Biol.* 134:971–983.

42. Zhong, M., W. Tian, …, J. I. Epstein. 2015. Distinguishing nested variants of urothelial carcinoma from benign mimickers by TERT promoter mutation. *Am. J. Surg. Pathol.* 39:127–131.

43. Fuchs, E., and D. W. Cleveland. 1998. A structural scaffolding of intermediate filaments in health and disease. *Science.* 279:514–519.

44. Coughlin, M. F., M. Puig-de-Morales, …, J. J. Fredberg. 2006. Filamin-a and rheological properties of cultured melanoma cells. *Biophys. J.* 90:2199–2205.

45. Dimitriadis, E. K., F. Horkay, …, R. S. Chadwick. 2002. Determination of elastic moduli of thin layers of soft material using the atomic force microscope. *Biophys. J.* 82:2798–2810.

46. Charras, G. T., and M. A. Horton. 2002. Determination of cellular strains by combined atomic force microscopy and finite element modeling. *Biophys. J.* 83:858–879.

47. Hu, S., J. Chen, …, N. Wang. 2003. Intracellular stress tomography reveals stress focusing and structural anisotropy in cytoskeleton of living cells. *Am. J. Physiol. Cell Physiol.* 285:C1082–C1090.

48. Tajik, A., Y. Zhang, …, N. Wang. 2016. Transcription upregulation via force-induced direct stretching of chromatin. *Nat. Mater.* 15:1287–1296.

49. Gruenbaum, Y., and U. Aebi. 2014. Intermediate filaments: a dynamic network that controls cell mechanics. *F1000Prime Rep.* 6:54.

50. Huber, F., A. Boire, …, G. H. Koenderink. 2015. Cytoskeletal crosstalk: when three different personalities team up. *Curr. Opin. Cell Biol.* 32:39–47.

51. Green, K. J., J. C. Talian, and R. D. Goldman. 1986. Relationship between intermediate filaments and microfilaments in cultured fibroblasts: evidence for common foci during cell spreading. *Cell Motil. Cytoskeleton.* 6:406–418.

52. Pesen, D., and J. H. Hoh. 2005. Micromechanical architecture of the endothelial cell cortex. *Biophys. J.* 88:670–679.

53. Eckes, B., D. Dogic, …, T. Krieg. 1998. Impaired mechanical stability, migration and contractile capacity in vimentin-deficient fibroblasts. *J. Cell Sci.* 111:1897–1907.

54. Wang, N., and D. Stamenović. 2000. Contribution of intermediate filaments to cell stiffness, stiffening, and growth. *Am. J. Physiol. Cell Physiol.* 279:C188–C194.

55. Mendez, M. G., D. Restle, and P. A. Janmey. 2014. Vimentin enhances cell elastic behavior and protects against compressive stress. *Biophys. J.* 107:314–323.

56. Sin, W. C., X. Q. Chen, …, L. Lim. 1998. RhoA-binding kinase alpha translocation is facilitated by the collapse of the vimentin intermediate filament network. *Mol. Cell. Biol.* 18:6325–6339.

57. Goto, H., H. Kosako, …, M. Inagaki. 1998. Phosphorylation of vimentin by Rho-associated kinase at a unique amino-terminal site that is specifically phosphorylated during cytokinesis. *J. Biol. Chem.* 273:11728–11736.

58. Inada, H., H. Togashi, …, M. Inagaki. 1999. Balance between activities of Rho kinase and type 1 protein phosphatase modulates turnover of phosphorylation and dynamics of desmin/vimentin filaments. *J. Biol. Chem.* 274:34932–34939.

59. Foley, K. S., and P. W. Young. 2014. The non-muscle functions of actinins: an update. *Biochem. J.* 459:1–13.

60. Kao, H. Y. 2015. The actinin family proteins: biological function and clinical implications. *Cell Biosci.* 5:48.

61. Inoue, T., and H. Tanihara. 2013. Rho-associated kinase inhibitors: a novel glaucoma therapy. *Prog. Retin. Eye Res.* 37:1–12.

62. Clark, A. F., K. Wilson, …, W. Howe. 1994. Glucocorticoid-induced formation of cross-linked actin networks in cultured human trabecular meshwork cells. *Invest. Ophthalmol. Vis. Sci.* 35:281–294.

63. Raghunathan, V. K., J. T. Morgan, …, P. Russell. 2015. Dexamethasone stiffens trabecular meshwork, trabecular meshwork cells, and matrix. *Invest. Ophthalmol. Vis. Sci.* 56:4447–4459.

64. Underwood, J. L., C. G. Murphy, …, J. A. Alvarado. 1999. Glucocorticoids regulate transendothelial fluid flow resistance and formation of intercellular junctions. *Am. J. Physiol.* 277:C330–C342.

65. Puig, F., N. Gavara, …, D. Navajas. 2009. Stiffening and contraction induced by dexamethasone in alveolar epithelial cells. *Exp. Mech.* 49:47–55.

66. Shah, V. P., C. C. Peck, and J. P. Skelly. 1989. 'Vasoconstriction'–skin blanching–assay for glucocorticoids–a critique. *Arch. Dermatol.* 125:1558–1561.

67. Becker, B. 1965. Intraocular pressure response to topical corticosteroids. *Invest. Ophthalmol.* 4:198–205.

68. Wu, P. H., D. R. Aroush, …, D. Wirtz. 2018. A comparison of methods to assess cell mechanical properties. *Nat. Methods.* 15:491–498.